Time-resolved infrared spectroscopy of molecule/binding site reorientation during ferroelectric liquid crystal electro-optic switching

Won Gun Jang, Cheol S. Park, and Noel A. Clark
Ferroelectric Liquid Crystal Materials Research Center, Department of Physics, University of Colorado, Boulder, Colorado 80309-0390
(Received 11 February 2000)

Polarized Fourier transform infrared (IR) absorption is used to probe molecular conformation in a ferroelectric liquid crystal during the large-scale collective reorientation induced by external applied electric field. Spectra of planar-aligned cells of the ferroelectric liquid crystal (FLC) **W314** ((S)-4′-(decyloxy)-4-[(1-methylheptyl)oxy]-2-nitrophenyl-[1,1'-biphenyl]-4-carboxylic acid ester) are measured as functions of IR polarizer orientation and time following the reversal of the electric field applied to the FLC. The time evolution of the dichroism of the absorbance due to the specific molecular vibration modes, particularly from the biphenyl core and alkyl tail, is observed. Static IR dichroism experiments show a **W314** IR dichroism structure in which the principal axis of the dielectric tensor from molecular core vibrations are tilted further from the smectic layer normal than those of the tail. This structure indicates that the effective binding site in which the molecules are confined in the Sm-C phase has, on average, a ''zig-zag'' shape. The dynamic experiments show that this zig-zag binding site structure is rigidly maintained while the molecular axis rotates about the layer normal during field-induced switching.

PACS number(s): 61.30.Gd, 78.30.Jw

I. INTRODUCTION

Infrared (IR) dichroism has proven to be a powerful probe of the molecular conformation and organization in liquid crystal phases. IR spectroscopy selects molecular vibrational modes, each of which has a transition dipole, fixed relative to the molecule or a molecular subfragment, which couples the vibration to incident IR light. Measurement of IR absorbance vs polarization orientation relative to the symmetry axes of a macroscopically single-domain sample then enables the moments of the transition dipole, and, therefore, of the molecular orientation distribution to be determined. It is particularly interesting to apply this technique to the lower symmetry liquid crystal (LC) phases, such as the smectic C (Sm-C), in which there is polar ordering of molecular subfragments, and the ferroelectric liquid crystal (FLC) chiral smectic C (Sm-C*), which is macroscopically polar. Recently Fourier transform IR (FTIR) studies of FLC's have probed the origin of polar ordering via static dichroism measurements [1,2], and molecular orientation during electric-field-induced switching via time-resolved spectroscopic (TRS) IR dichroism measurements [3,4,5,6], studying in particular, the relative motion of major molecular subfragments [7,8,9,10]. Here we present the first dynamical studies probing the mean molecular geometry during electric-field-induced reorientation.

Macroscopic polar ordering in liquid crystals (LC's) was discovered in the chiral smectic C (Sm-C*) liquid crystal **DOBAMBC** by Meyer *et al.* [11] and has been intensively studied since the demonstration of ferroelectric domains and fast, bistable electro-optic effects in the bookshelf surface-stabilized ferroelectric (SSFLC) cell geometry of Fig. 1 [12]. Sm-C* liquid crystals are fluid ferroelectrics, characterized by the structure shown in Fig. 1, a one-dimensional (1D) stacking of 2D liquid layers of rod-shaped molecules having a mean long molecular axis (optic axis) tilted through a fixed angle θ from the layer normal. Such a phase is required by the chiral symmetry to have a macroscopic spontaneous ferroelectric polarization $\mathbf{P}_s$, locally normal to the mean long axis **n** and to the layer normal **z**. Although the magnitude of $\mathbf{P}_s$ is fixed, depending only on temperature, the azimuthal orientation $\phi(\mathbf{r})$ responds to applied electric field, surface interactions, and elasticity of the director field, $\mathbf{n}(\mathbf{r})$. For a square-wave voltage of sufficiently large amplitude applied to the cell geometry of Fig. 1, $\mathbf{n}(\mathbf{r})$ is spatially uniform and is

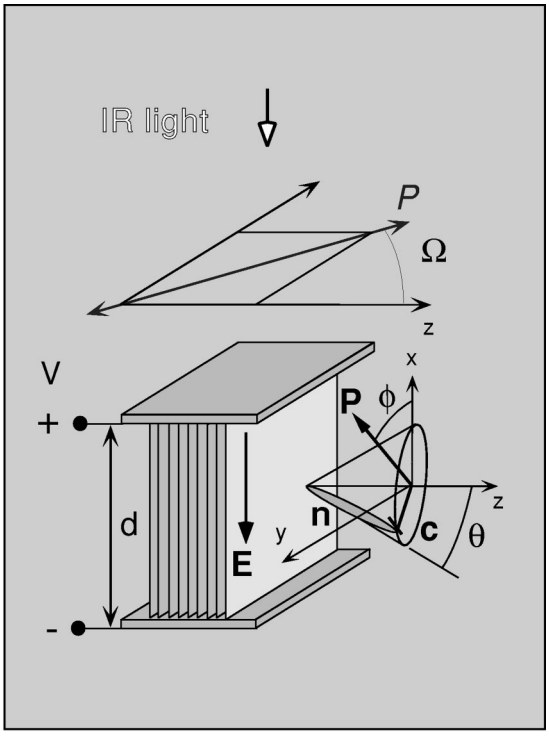

FIG. 1. A schematic diagram of the FTIR experiment.

 ©2000 The American Physical Society

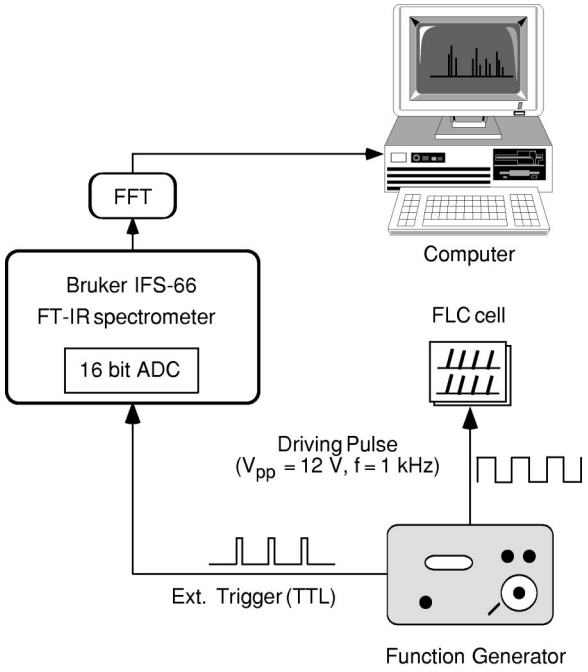

FIG. 2. FTIR time-resolved spectroscopy setup. A 1 KHz 12 V_{pp} square wave is applied to the FLC cell and synchronized TTL trigger pulse signals for data sampling are fed onto the 16-bit analog-to-digital converter of the main spectrometer. Spectrometer transmission is collected while both interferometer path difference and time delay following reversal of the voltage on the FLC cell are changing. Thirty independent measurements are made at each mirror position and time delay. The computer then sorts, averages, and Fourier transforms the data to obtain spectra vs time delay.

driven by the field around on the tilt cone, saturating at $\phi = 0$ for $V>0$ and at $\phi=\pi$ for $V<0$. This cell geometry is also very useful for probing the response of molecular orientation to applied field via IR dichroism, with the IR light incident along **x**, normal to the cell [7]. With field applied the Sm-C* **n-z** tilt plane is normal to the incident IR light, so that by varying the IR polarization one can then probe the orientation of the absorption dipoles in the tilt plane.

II. EXPERIMENT

The experimental cell geometry is represented in Fig. 1 and the electronic setup shown in Fig. 2. Step-scan FTIR time-resolved spectroscopy (TRS) is conducted using a Bruker IFS 66 FTIR Michelson interference spectrometer. A photovoltaic mercury cadmium telluride detector with a 50 MHz preamplifier (Kolmar Technology) and an internal analog to digital converter (ADC) board is used to detect the modulated IR signal. A square wave voltage is applied to the liquid crystal cell using a function generator ($V_{pp}=12$ V), and synchronized transistor and transistor lock (TTL) trigger pulse signals for data sampling are fed onto the 16-bit analog-to-digital converter of the main spectrometer. Spectrometer transmission is collected while both interferometer path difference and time delay following reversal of the voltage on the FLC cell are evolving. Thirty independent measurements are made at each mirror position and time delay. The computer then sorts, averages, and Fourier transforms the data to obtain spectra vs time delay. Raw spectra are then

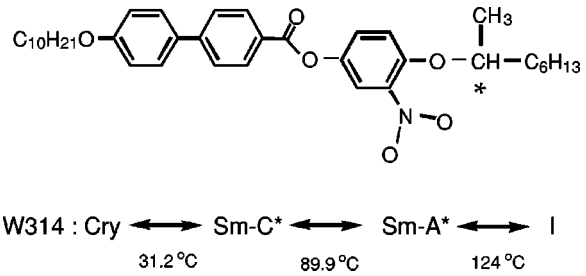

FIG. 3. Phase diagram and chemical structure of ferroelectric liquid crystal compound **W314**.

baseline corrected and values of absorbance peaks determined. Data are presented here for peaks at 2927, 1736, 1606, and 1535 cm^{-1}, due to the *alkyl* tail, *carbonyl* group, *phenyl* core, and *nitro* group stretching modes, respectively. A wire-grid IR polarizer is positioned between the IR source and the sample and its orientation Ω is set at 10° intervals under computer control, with $\Omega=0°$ having IR polarization parallel to layer normal. Spectra are measured for the full range of time delay for each setting of Ω. Spectra were recorded at 4 cm^{-1} spectral resolution in consecutive time series of 5 μs intervals up to a maximum delay after reversal of 500 μs, limited by the applied frequency of 1 kHz.

W314, shown in Fig. 3 along with its phase diagram, was obtained from D. M. Walba. **W314** has negative spontaneous polarization of large magnitude ($0<|\mathbf{P}_s|<426$ nC/cm^2), which is mainly due to the electronegative constituent $-NO_2$ [13]. The electro-optic cells were IR and visible light transparent capacitors made from CaF_2 windows coated with a thin layer of indium-tin oxide (ITO) for electrodes and spaced to a LC thickness of 2–3 μm by uniform polymer balls. The ITO was spin coated with a 200 Å thick nylon film which was buffed using a rotating brush to align the LC. The cells were filled with W314 in the isotropic phase and cooled slowly into the Sm-A* and Sm-C* phases. Alignment quality was checked with visible light polarized microscopy. The layer structure obtained upon cooling into the Sm-C* phase was a chevron, but the voltage threshold for deforming the chevron structure into the bookshelf was quite low (several volts), so that the IR experiments were always carried out in the bookshelf geometry, i.e., with the smectic layers normal to the plates.

Initial evaluation of a cell and its time response was obtained in the Sm-C* phase by setting $\Omega\approx\theta$ such that the IR polarization vector is parallel to liquid crystal director, **n**, with one sign of voltage applied to the cell. Field reversal then produces a reorientation of $\sim 2\theta$ of **n**, giving clear absorption changes. Figure 4 shows such data taken in the Sm-C* phase at $T=70$ °C, where $\theta=28.9°$. The transient reorientation and its saturation is evident in the four distinct vibrational modes studied. The change in absorbance observed can be qualitatively understood for each mode in terms of β, the angle between its absorption dipole and the molecular long axis; The *phenyl* core vibration has $\beta\sim 0°$, and thus the largest change in absorbance, the *alkyl* CH_2 stretching vibration has $\beta\sim 90°$, for an all-trans tail, with the change in absorbance being reduced because of disorder in the tails; The *nitro* stretching vibration has $\beta\sim 30°$; and the *carbonyl* stretching vibration has $\beta\sim 60°$ and shows a small change in absorbance because this β is close to the ''magic

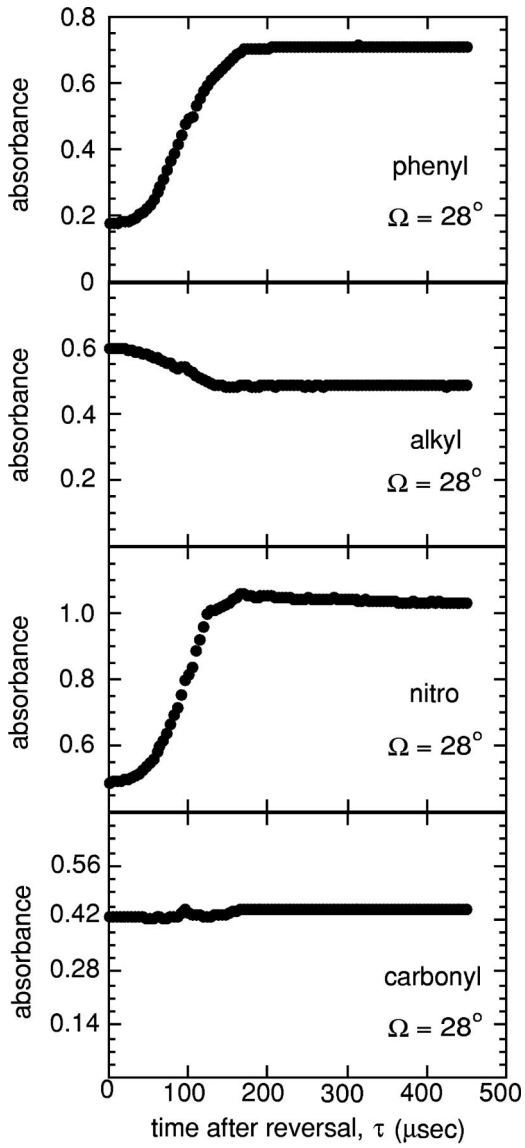

FIG. 4. Absorbance changes upon field reversal for the phenyl, alkyl, NO_2, and C=O group modes at $T=70°C$. Half of the total change of absorbance of the *phenyl* mode is reached in 90 μs and full absorbance is reached in 200 μsec. The time response for the *nitro* and *alkyl* modes are similar, indicating that the molecule binding site reorients as a rigid unit. The carbonyl mode shows little change in absorbance because its transition moment orientation relative to the molecular long axis is close to the ''magic angle.''

angle,'' $\beta=54.7°$, for which a uniaxial distribution about the long axis appears isotropic.

It is not possible to extract molecular orientation parameters from data, as in Fig. 4, at a single polarizer orientation Ω. Hence for full data analysis time-resolved peak absorbance for each vibration is obtained by fits to the spectra for a series of Ω, spaced by 10° intervals. The results are displayed in Fig. 5 as polar plots of peak absorbance $A(\Omega)$, which effectively exhibit the dichroism of each mode, and its evolution with time. Ignoring birefringence [14], $A(\Omega)$ for any mode must be of the form (1)

$$A(\Omega)=-\log\{(10^{-A_{para}})\cos^2(\Omega-\Omega_0)+(10^{-A_{perp}})\sin^2(\Omega-\Omega_0)\}, \quad (1)$$

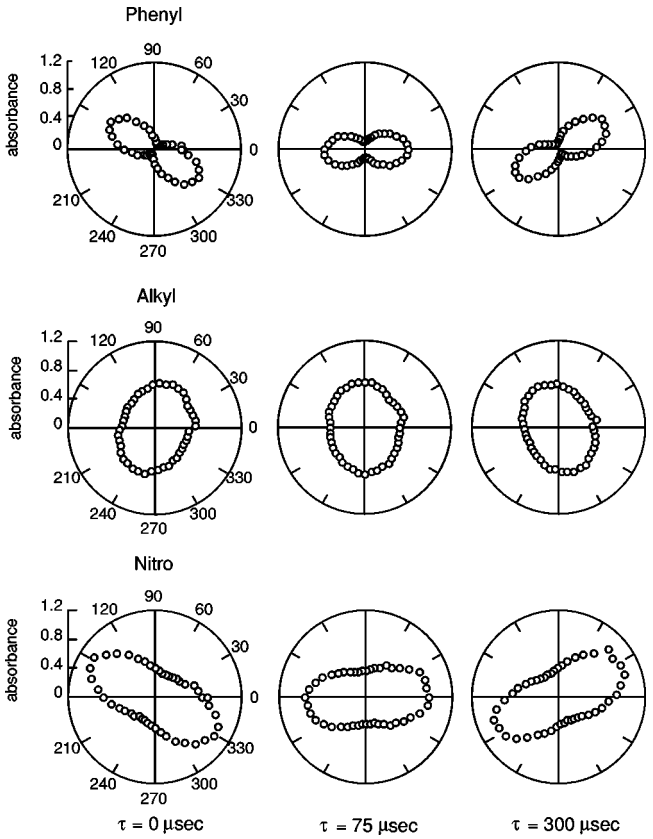

FIG. 5. Polar plots of IR absorbance vs IR polarizer orientation Ω for (a) 0 μs (b) 75 μs and (c) 300 μs time delay following field reversal at $T=70°C$. Field-induced reorientations of phenyl core and alkyl tail start from $-28.9°$ and $-24.2°$ to 28.9° and 23.9°, respectively, and complete in 200 μs after switching starts.

where the absorbances A_{para} (A_{perp}) are those measured with the IR polarizer parallel (perpendicular) to the $\Omega=\Omega_0$ axis, the polarizer orientation for either maximum (A_{max}) or minimum (A_{min}) absorbance [1]. Polar plots of $A(\Omega)$ for the *phenyl*, *alkyl*, and *nitro* modes for time after field reversal $\tau=0$, 75, and 300 μs are shown in Fig. 5. The reorientation of Ω_0 with field reversal is evident.

III. RESULTS AND DISCUSSION

Fits of Eq. (1) to $A(\Omega)$ data enables the determination of Ω_0 vs τ, with the result shown in Fig. 6(a) for the *phenyl* and *nitro* (core) and *alkyl* (tail) vibrations, Ω_0 giving the IR polarizer orientation of A_{max} (A_{min}) for the *phenyl* and *nitro* (*alkyl*) vibrations. As can be seen, while the dynamics of the core and tail appear to be similar, there is a marked difference between the asymptotic $\Omega_0(T)_{phenyl}\equiv\Omega_0(T,\tau\rightarrow\infty)_{phenyl}$, and $\Omega_0(T)_{alkyl}\equiv\Omega_0(T,\tau\rightarrow\infty)_{alkyl}$, with the net reorientation of the *phenyl* vibration considerably larger than that of the other modes. Figure 6(b) shows the time dependence of $\Delta\Omega_0(T,\tau)\equiv\Omega_0(T,\tau)_{phenyl}-\Omega_0(T,\tau)_{alkyl}$, the difference in Ω_0 for the *phenyl* and *alkyl* vibrations at $T=70$ °C, which has a time dependence similar to that of $\Omega_{\bigcirc}(T,\tau)_{phenyl}$ and $\Omega_0(T,\tau)_{alkyl}$ themselves. The asymptotic values $\Omega_0(T)_{phenyl}$ and $\Omega_0(T)_{alkyl}$ and their difference are consistent with the results from static dichroism measurements [15], shown in Fig. 7. Here we plot

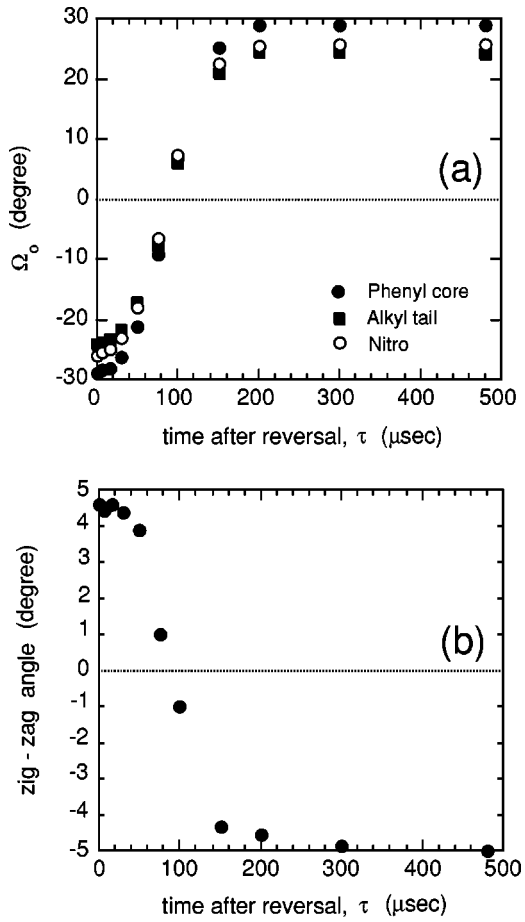

FIG. 6. (a) Time dependence following field reversal of $\Omega_0(\tau)$, the IR polarizer orientation of A_{max} (A_{min}) for the *phenyl* and *nitro* (*alkyl*) vibrations. The three modes show similar time dependence, suggesting rigid rotation of the molecular binding site, but have different asymptotic values, $\Omega_0(\tau\rightarrow\infty)$, indicative of a zig-zag molecular structure with the tails less tilted than the cores. (b) Time dependence of the ''zig-zag'' angle $\Delta\Omega_0(T,\tau)\approx\Omega_0(T,\tau)_{phenyl}-\Omega_0(T,\tau)_{alkyl}$.

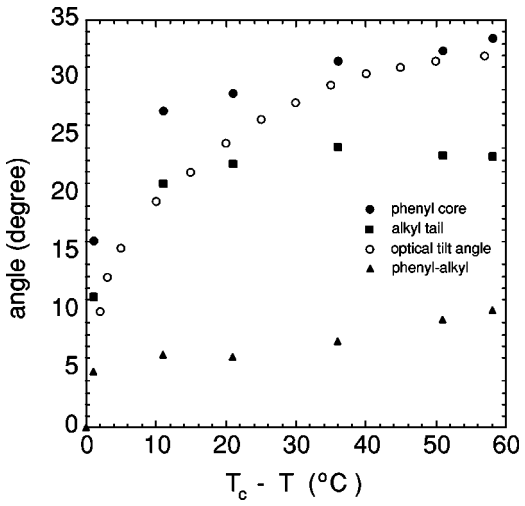

FIG. 7. Static measurements of the IR polarizer orientation of A_{max} (A_{min}) for the *phenyl* (*alkyl*) vibrations vs T, along with their difference, $\Delta\Omega_0(T)\approx\Omega_0(T)_{phenyl}-\Omega_0(T)_{alkyl}$, and visible light optic axis tilt data. The dynamic measurements were carried out at $T=70°$C.

the visible light optical axis tilt relative to the layer normal θ(T), along with $\Omega_0(T)_{phenyl}$ and $\Omega_0(T)_{alkyl}$, and their difference $\Delta\Omega_0(T)=\Omega_0(T)_{phenyl}-\Omega_0(T)_{alkyl}$. The dynamic IR measurements reported here have been carried out at $T=70$ °C and 40 °C, at which $\Delta\Omega_0(T)\sim 6°$ and 9°, respectively.

The three parameters A_{max}, A_{min}, and Ω_0 are related to $\langle p_i p_j\rangle_m$ the moments of the orientation distribution of the mode absorption dipole **p**, which is proportional to the imaginary part of the contribution of the mode to the dielectric tensor, $(\delta\varepsilon_{ij})_m\propto\langle p_i p_j\rangle_m$. The Ω_0 axis is the projection, onto the **y**-**z** plane of polarization of the IR light, of a principal axis of $\langle p_i p_j\rangle_m$ or $(\delta\varepsilon_{ij})_m$. In the static Sm-C or Sm-C* phase, the coordinate system which diagonalizes the matrix $\langle p_i p_j\rangle$ has one axis parallel to the twofold rotation axis, i.e., parallel to the polarization $\mathbf{P}_s$ in a Sm-C* phase, and has the other two axes in the Sm-C tilt plane, normal to $\mathbf{P}_s$. Thus with the field applied in the geometry of Fig. 1, $\langle p_x p_z\rangle=\langle p_x p_y\rangle=0$, and $A(\Omega)$ is determined by the three moments, $\langle p_y^2\rangle$, $\langle p_z^2\rangle$, and $\langle p_y p_z\rangle$, of the orientation distribution. Since the transition dipole for the *phenyl* transition is parallel to the core, the coordinate system diagonalizing $\langle p_i p_j\rangle_{phenyl}$ has an axis parallel to the core, and $\Omega_0(T)_{phenyl}$ is a measure of the mean core orientation projected onto the tilt plane. Additionally, since the transition dipole for the *alkyl* transition is normal to an extended all-trans chain, the coordinate system diagonalizing $\langle p_i p_j\rangle_{alkyl}$ has an axis parallel to an extended tail, and $\Omega_0(T)_{alkyl}$ is a measure of the mean tail orientation projected onto the tilt plane. Thus, the finite $\Delta\Omega_0$ indicates that the molecular organization in the phase has the tails less tilted on average than the cores, by the angle $\Delta\Omega_0$ which approaches 10° in Sm-C* at low T, and thus that the mean molecular configuration is bent. Since $\Omega_0(T)_{phenyl}$ is a good measure of the actual core tilt, it is comparable to the optic axis tilt, which is determined largely by the optical anisotropy of the core, with a principal axis also at nearly $\Omega_0(T)_{phenyl}$. The optic axis orientation is, in Fig. 7, slightly smaller than $\Omega_0(T)_{phenyl}$, possibly because of the contribution of the tails to the birefringence. This larger tilt of the cores relative to the tails is a generic feature of the Sm-C phase, first analyzed by Durand and co-workers [16], who noted that it leads to less layer shrinkage in the Sm-C phase, as measured by x-ray diffraction, than expected on the basis of the optic axis tilt [17], determined primarily by the core.

Given the Sm-*C* two fold axes, parallel to **x** in the layer midplanes, the mean molecular organization with the tails less tilted than the cores implies that the molecular mean field or binding site imposed on a molecule by its neighbors is zig-zag-shaped (a zig-zag bent cylindrical hole), and leads to a natural explanation of the polar ordering about the molecular long axis in the Sm-C phase, since, in general, only a single orientation of a bent molecular conformation about its long axis will minimize energy in a zig-zag shaped binding site. Thus the ferroelectric polarization is determined by the equilibrium distribution of bent molecular conformers in an ensemble of zig-zag binding sites (the Boulder model [18]). This kind of mean-field picture leads to a technique for prediction of the ferroelectric polarization, using atomistic simulation to equilibrate single molecules in zig-zag mean-

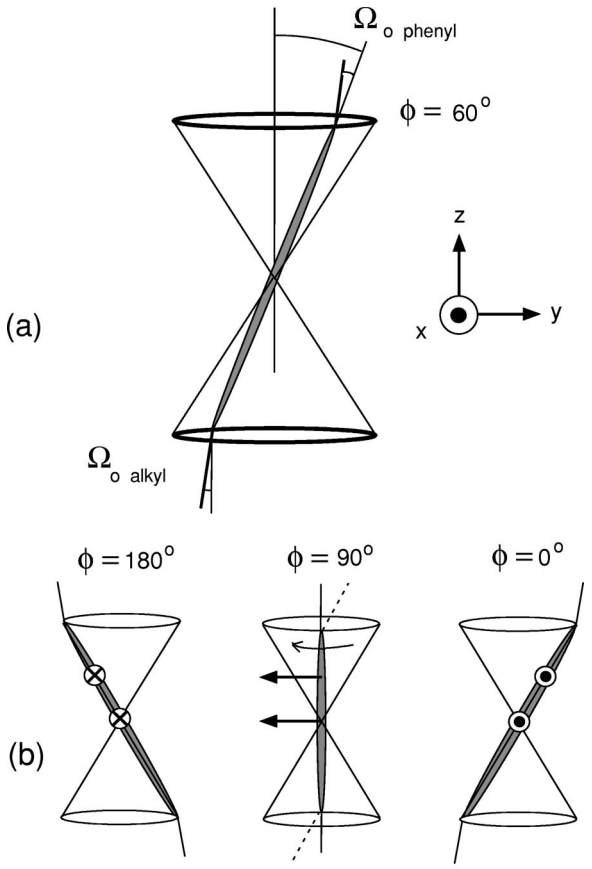

FIG. 8. Schematic of the zig-zag structure of the Sm-C binding site and the field-induced rotation on the tilt cone. The IR dynamics data indicate a rigid rotation on the cone, with core and tail in the same (rotating) tilt plane with a fixed zig-zag angle. If the tails are pulled around by the core during field-induced motion on the core, then the dashed tail configuration would develop.

field potentials [19], which is quite successful for **W314** and its nitroalkoxy homologs. Note that for molecules which have two similar length alkyl tails a smaller mean tail tilt indicates unambiguously a zig-zag molecular shape, as indicated in Fig. 8 in the Sm-C phase. For molecules with distinctly different tail lengths, such as **W314**, the overall molecular shape indicated by a smaller mean tail tilt is less obvious, as short tails can orient in a variety of ways. For example, in **MHPOBC**, the molecule has a distinct 90° bend at the methyl hepty oxy tail [20].

Figure 8 is a sketch of the generic equilibrium Sm-C structure, representing either the molecular binding site (the mean hole in which molecules are confined), or the mean molecular structure of a pair of molecules related by the Sm-C two-fold axis along **x**. In equilibrium the tail (stick) and core (ellipse) components of the binding site are in the Sm-C (**y**-**z**) tilt plane. This may no longer be the case during switching if the core and tail reorientation dynamics are different. For example, if the tails are dragged around by the core, the dashed tail orientation of Fig. 8(b) would obtain, and $\Omega_0(t)_{alkyl}$ would be nonzero when $\Omega_0(t)_{phenyl} = 0$. In order to check for such an effect we first assume that it does not exist and that the principal axes of the *phenyl* and *alkyl* moments remain in a common plane (the Sm-C tilt plane) throughout the reorientation. The $\Omega_0(\tau)_{phenyl}$ and $\Omega_0(\tau)_{alkyl}$

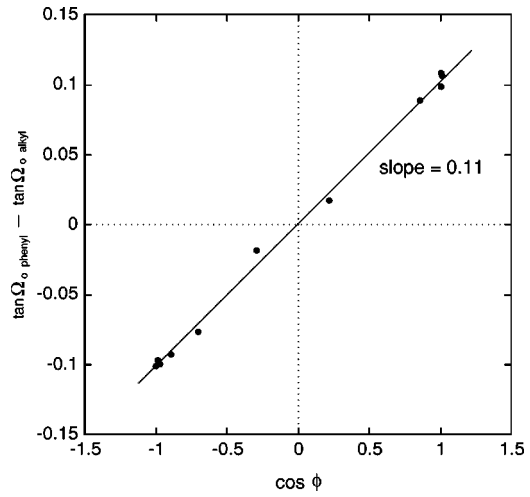

FIG. 9. Plot of $\tan\Omega_0(\tau)_{phenyl} - \tan\Omega_0(\tau)_{alkyl}$ vs $\cos\phi$, fitted to the straight line through the origin predicted for rigid molecular reorientation. The fitted slope $S = 0.11$ is agreement with the predicted $S = \tan\Omega_0(T)_{phenyl} - \tan\Omega_0(T)_{alkyl} = 0.122$, obtained from the static data of Fig. 7 within error.

are just the respective projections of these principal axes onto the **y**- **z** plane. The geometry in Fig. 8 gives

$$\Omega_0(\tau) = \arctan\frac{\sin\Omega_0(\tau\rightarrow\infty)\cos\phi}{\cos\Omega_0(\tau\rightarrow\infty)}, \tag{2}$$

and

$$\begin{aligned}\tan\Omega_0(\tau)_{phenyl} - \tan\Omega_0(\tau)_{alkyl} &= \{\tan\Omega_0(\tau\rightarrow\infty)_{phenyl} - \tan\Omega_0(\tau\rightarrow\infty)_{alkyl}\}\cos\phi \\ &= \{\tan\Omega_0(T)_{phenyl} - \tan\Omega_0(T)_{alkyl}\}\cos\phi. \end{aligned}\tag{3}$$

Thus the signature of rigid rotation of the zig-zag structure is a linear variation of $\{\tan\Omega_0(\tau)_{phenyl} - \tan\Omega_0(\tau)_{alkyl}\}$ with $\cos\phi$, which, as Fig. 9 shows, fits the data well. The fitted slope $S = 0.11$ agrees within error with the expected value $S = \{\tan\Omega_0(T)_{phenyl} - \tan\Omega_0(T)_{alkyl}\} = 0.122$, obtained from the static data of Fig. 7.

Figure 4 shows that the dichroism of the phenyl is lower for $\phi \approx 90°$ ($\tau \approx 75\ \mu$s), than for $\phi \approx 0°$ ($\tau \approx 0\ \mu$s), or $\phi \approx 180°$ ($\tau \approx 300\ \mu$s), a result of a reduced A_{max} and increased A_{min} at $\phi \approx 90°$. The tipping of the core away from the **y**-**z** plane at $\phi = 90°$ (see Fig. 8) contributes partly to this change, reducing A_{max}. The increased A_{min} is due to the anisotropy in the orientation fluctuations of the core, the fluctuations being larger in the ϕ direction than in the θ direction.

IV. CONCLUSION

We confirm, using time-resolved IR spectroscopy, that the response of Sm-C* **W314** to field reversal is polarization reversal via field-induced rotation of the molecular director around on the Sm-C* tilt cone. During this rotation the dynamics of the molecular core and tail segments is identical in the sense that the average molecular conformation appears to rotate on the cone as a rigid unit, with both tail and core transition moment axes confined to the same (rotating) tilt

plane (passing through the layer normal projection at the same time) and keeping a fixed relative tilt (zig-zag) angle. These results may be compared to those of other FTIR TRS studies of macroscopic field-induced director reorientation. In field-driven reorientation of FLC side chain siloxane polymers and dimers [9,10] similar reorientational rates for the core and tail are found. However, in the (electroclinic) field-induced director rotation in the Sm-A phase of **W317** [7], the core and tail segments respond differently to applied field, the tail motion delayed relative to the core. Changes in absorbance suggesting tail motion preceding that of the core has been found in nematic reorientation, although not via analysis of the $\Omega_0(\tau)$ time dependence [21]. The origin of these differences is unclear at this point. However, a general direction for effectively probing the dynamics is clear, specifically to apply larger voltage transients to drive the reorientation faster. One might expect that time delay in the relative motion of different subfragments, if observed, would be independent of the overall switching time, and thus would show up more distinctly with fast switching than with slow. Interestingly, nematics, where the field-induced switching times decrease as applied field E^{-2}, appear to be the best candidates for fast field-switching FTIR TRS experiments.

ACKNOWLEDGMENTS

This work was supported by NSF MRSEC Grant No. DMR 98-09555, ARO Grant No. DAAG55-98-1-0046, and AFOSR MURI F49620-97-1-0014.

[1] W. G. Jang, C. S. Park, J. E. Maclennan, K. H. Kim, and N. A. Clark, Ferroelectrics **180**, 213 (1996).
[2] K. H. Kim, K. Ishikawa, H. Takezoe, and A. Fukuda, Phys. Rev. E **51**, 2166 (1995).
[3] W. Uhmann, A. Becker, C. Taran, and F. Siebert, Appl. Spectrosc. **45**, 390 (1991).
[4] K. Masutani, H. Sugisawa, A. Yokota, Y. Furukawa, and M. Tasumi, Appl. Spectrosc. **46**, 560 (1992).
[5] R. A. Palmer, J. L. Chao, R. M. Dittmar, V. G. Gregoriou, and S. E. Plunkett, Appl. Spectrosc. **47**, 1297 (1993).
[6] T. Nakano, T. Yokoyama, and H. Toriumi, Appl. Spectrosc. **47**, 1354 (1993).
[7] F. Hide, N. A. Clark, K. Nito, A. Yasuda, and D. M. Walba, Phys. Rev. Lett. **75**, 2344 (1995).
[8] S. V. Shilov, H. Skupin, F. Kremer, T. Wittig, and R. Zentel, FTS/IR Notes No. 105, Biorad Corporation, Cambridge, MA, 1996.
[9] S. V. Shilov, H. Skupin, F. Kremer, E. Gebhard, and R. Zentel, Liq. Cryst. **22**, 203 (1997).
[10] S. V. Shilov, H. Skupin, F. Kremer, T. Wittig, and R. Zentel, Phys. Rev. Lett. **79**, 1686 (1997).
[11] R. B. Meyer, L. Liebert, L. Strzelecki, and P. Keller, J. Phys. (France) **36**, L-69 (1975).
[12] N. A. Clark and S. T. Lagerwall, Appl. Phys. Lett. **36**, 899 (1980).
[13] D. M. Walba, M. B. Ros, N. A. Clark, R. Shao, M. G. Robinson, J. Y. Liu, K. M. Johnson, and D. Doroski, J. Am. Chem. Soc. **113**, 5471 (1991).
[14] Equation (1) is exact only in the absence of birefringence (optical anisotropy in the real part of the dielectric constant), when the eigenmodes of a dichroic medium are linearly polarized along the directions of maximum and minimum absorbance. For the vibrations studied here, polarized nearly along the optic axis of the real part of the dielectric constant, the birefringence can be ignored in few micron thick samples.
[15] W. G. Jang, M. Glaser, C. S. Park, K. H. Kim, and N. A. Clark (unpublished).
[16] R. Bartolino, J. Doucet, and G. Durand, Ann. Phys. (N.Y.) **3**, 389 (1978).
[17] T. P. Rieker, N. A. Clark, G. S. Smith, D. S. Parmar, E. B. Sirota, and C. R. Safinya, Phys. Rev. Lett. **59**, 2658 (1987); N. A. Clark and T. P. Rieker, Phys. Rev. A **39**, 5450 (1989).
[18] D. M. Walba and N. A. Clark, Ferroelectrics **84**, 65 (1988).
[19] M. A. Glaser, V. V. Ginzburg, N. A. Clark, E. Garcia, D. M. Walba, and R. Malzbender, Mol. Phys. Rep. **10**, 26 (1995).
[20] B. Jin, Z. Ling, Y. Takanishi, K. Ishikawa, H. Takezoe, A. Fukuda, M. Kakimoto, and T. Kitazume, Phys. Rev. E **53**, R4295 (1996).
[21] T. Urano and H. Hamaguchi, Chem. Phys. Lett. **195**, 287 (1992).